

2014

Internal stress-induced melting below melting temperature at high-rate laser heating

Yong Seok Hwang
Iowa State University

Valery I. Levitas
Iowa State University, vlevitas@iastate.edu

Follow this and additional works at: http://lib.dr.iastate.edu/aere_pubs



Part of the [Structures and Materials Commons](#)

The complete bibliographic information for this item can be found at http://lib.dr.iastate.edu/aere_pubs/98. For information on how to cite this item, please visit <http://lib.dr.iastate.edu/howtocite.html>.

This Article is brought to you for free and open access by the Aerospace Engineering at Iowa State University Digital Repository. It has been accepted for inclusion in Aerospace Engineering Publications by an authorized administrator of Iowa State University Digital Repository. For more information, please contact digirep@iastate.edu.

Internal stress-induced melting below melting temperature at high-rate laser heating

Abstract

In this Letter, continuum thermodynamic and phase field approaches (PFAs) predicted internal stress-induced reduction in melting temperature for laser-irradiated heating of a nanolayer. Internal stresses appear due to thermal strain under constrained conditions and completely relax during melting, producing an additional thermodynamic driving force for melting. Thermodynamic melting temperature for Al reduces from 933.67 K for a stress-free condition down to 898.1 K for uniaxial strain and to 920.8 K for plane strain. Our PFA simulations demonstrated barrierless surface-induced melt nucleation below these temperatures and propagation of two solid-melt interfaces toward each other at the temperatures very close to the corresponding predicted thermodynamic equilibrium temperatures for the heating rate $Q \leq 1.51 \times 10^{10} \text{K/s}$. At higher heating rates, kinetic superheating competes with a reduction in melting temperature and melting under uniaxial strain occurs at 902.1 K for $Q = 1.51 \times 10^{11} \text{K/s}$ and 936.9 K for $Q = 1.46 \times 10^{12} \text{K/s}$.

Disciplines

Aerospace Engineering | Structures and Materials

Comments

This article is published as Hwang, Yong Seok, and Valery I. Levitas. "Internal stress-induced melting below melting temperature at high-rate laser heating." *Applied Physics Letters* 104, no. 26 (2014): 263106. doi: [10.1063/1.4886799](https://doi.org/10.1063/1.4886799). Posted with permission.

Internal stress-induced melting below melting temperature at high-rate laser heating

Yong Seok Hwang, and Valery I. Levitas

Citation: *Appl. Phys. Lett.* **104**, 263106 (2014);

View online: <https://doi.org/10.1063/1.4886799>

View Table of Contents: <http://aip.scitation.org/toc/apl/104/26>

Published by the [American Institute of Physics](#)

Articles you may be interested in

[Phase field simulation of kinetic superheating and melting of aluminum nanolayer irradiated by pico- and femtosecond laser](#)

Applied Physics Letters **103**, 263107 (2013); 10.1063/1.4858395

[Effect of stress on melting of rhombohedral bismuth](#)

Applied Physics Letters **110**, 161904 (2017); 10.1063/1.4981810

[Developments in time-resolved high pressure x-ray diffraction using rapid compression and decompression](#)

Review of Scientific Instruments **86**, 072208 (2015); 10.1063/1.4926887

[Online remote control systems for static and dynamic compression and decompression using diamond anvil cells](#)

Review of Scientific Instruments **86**, 072209 (2015); 10.1063/1.4926892

[New developments in micro-X-ray diffraction and X-ray absorption spectroscopy for high-pressure research at 16-BM-D at the Advanced Photon Source](#)

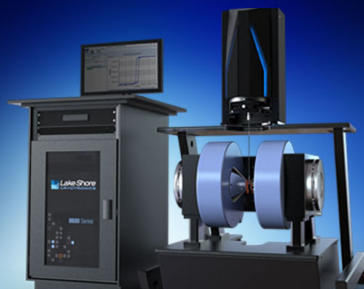
Review of Scientific Instruments **86**, 072205 (2015); 10.1063/1.4926893

[Internal stresses in pre-stressed micron-scale aluminum core-shell particles and their improved reactivity](#)

Journal of Applied Physics **118**, 094305 (2015); 10.1063/1.4929642




Lake Shore
CRYOTRONICS



8600 Series VSM

For fast, highly sensitive
measurement performance

LEARN MORE 

Internal stress-induced melting below melting temperature at high-rate laser heating

Yong Seok Hwang^{1,a)} and Valery I. Levitas^{2,b)}

¹Department of Aerospace Engineering, Iowa State University, Ames, Iowa 50011, USA

²Departments of Aerospace Engineering, Mechanical Engineering, and Material Science and Engineering, Iowa State University, Ames, Iowa 50011, USA

(Received 2 May 2014; accepted 20 June 2014; published online 2 July 2014)

In this Letter, continuum thermodynamic and phase field approaches (PFAs) predicted internal stress-induced reduction in melting temperature for laser-irradiated heating of a nanolayer. Internal stresses appear due to thermal strain under constrained conditions and completely relax during melting, producing an additional thermodynamic driving force for melting. Thermodynamic melting temperature for Al reduces from 933.67 K for a stress-free condition down to 898.1 K for uniaxial strain and to 920.8 K for plane strain. Our PFA simulations demonstrated barrierless surface-induced melt nucleation below these temperatures and propagation of two solid-melt interfaces toward each other at the temperatures very close to the corresponding predicted thermodynamic equilibrium temperatures for the heating rate $Q \leq 1.51 \times 10^{10}$ K/s. At higher heating rates, kinetic superheating competes with a reduction in melting temperature and melting under uniaxial strain occurs at 902.1 K for $Q = 1.51 \times 10^{11}$ K/s and 936.9 K for $Q = 1.46 \times 10^{12}$ K/s. © 2014 AIP Publishing LLC.

[<http://dx.doi.org/10.1063/1.4886799>]

Traditionally, intense laser-induced melting is associated with the possibility of significant kinetic superheating of solids and their melting significantly above the equilibrium melting temperature T_{eq} . This was obtained experimentally for heating rates Q in the range 0.95–1290 K/ps,^{1,2} using molecular dynamics³ and phase field approach (PFA).⁴ For example, for the heating rate $Q = 1290$ K/ps, experimental² melting temperature for Al increased up to 1400 K, while $T_{eq} = 933.67$ K. Such fast heating leads to a high temperature T before melting starts and completes. Also, thermal expansion in constraint conditions generates compressive pressure, which is supposed to increase the equilibrium melting temperature according to Clausius-Clapeyron relation. We are not familiar of experimental or numerical studies of melting under laser heating for smaller $Q < 10^{11}$ K/s. Here, we demonstrate that laser heating in a broad range of heating rates $Q < 10^{11}$ K/s can cause melting at 36 K, *below the equilibrium melting temperature* of Al at zero external pressure in biaxial confinement. The main reason of reducing melting temperature is that fast heating within a laser-irradiated region of a thin nanolayer generates constrained thermal expansion and *internal* elastic biaxial compression on the order of 2 GPa without external pressure. Using continuum thermodynamics, we demonstrated analytically that such internal stresses and their energy, which completely relax after melting, produce a significant driving force for melting and reduce equilibrium melting temperature T_{eq}^e by 36 K. The same reduction in actual melting temperature was obtained utilizing advanced PFA coupled to mechanics and the heat evolution equation. When mechanics is excluded, melting occurs at equilibrium temperature T_{eq} . At higher heating rates, this driving force still persists but kinetic superheating

takes over, leading to a significant increase in melting temperature with respect to T_{eq}^e .

Phase field equations. We will generalize the phase field approach for melting coupled with mechanics developed in Refs. 4–6 by adding a thermodynamically consistent temperature evolution equation. Since these equations describe well experimental results, for surface melting and melting of Al nanoparticles at slow heating⁶ and melting at laser heating of the thin Al nanolayer (like here), for $Q = 0.95$ –1290 K/ps,⁴ we expect that they describe reality for the heating rates in the current paper.

Total strain tensor $\boldsymbol{\varepsilon} = (\nabla_0 \mathbf{u})_s$ (where \mathbf{u} is the displacement vector, ∇_0 is the gradient operator in the undeformed state, and the subscript s designates symmetrization) can be additively decomposed into elastic $\boldsymbol{\varepsilon}_e$, transformation $\boldsymbol{\varepsilon}_t$, and thermal $\boldsymbol{\varepsilon}_\theta$ strains

$$\boldsymbol{\varepsilon} = \boldsymbol{\varepsilon}_e + \boldsymbol{\varepsilon}_t + \boldsymbol{\varepsilon}_\theta; \quad \boldsymbol{\varepsilon} = 1/3\varepsilon_0 \mathbf{I} + \mathbf{e}; \quad (1)$$

$$\boldsymbol{\varepsilon}_{in} = \varepsilon_{in} \mathbf{I} = \boldsymbol{\varepsilon}_t + \boldsymbol{\varepsilon}_\theta; \quad \boldsymbol{\varepsilon}_t = 1/3\varepsilon_{0t}(1 - \phi(\eta)) \mathbf{I}; \quad (2)$$

$$\boldsymbol{\varepsilon}_\theta = \alpha_s(T_{eq} - T_0) \mathbf{I} + (\alpha_m + \Delta\alpha\phi(\eta))(T - T_{eq}) \mathbf{I}, \quad (3)$$

where η is the order parameter that varies from 1 in solid to 0 in melt and characterizes the degree of disordering of atomic structure, α_s and α_m are the linear thermal expansion coefficients for solid and melt, respectively, $\Delta\alpha$ is the difference in the thermal expansion coefficients of solid and melt, \mathbf{I} is the unit tensor, T_0 is the initial temperature, ε_0 is the total volumetric strain, ε_{0t} is the volumetric transformation strain for complete melting, \mathbf{e} is the deviatoric strain, and $\phi(\eta) = \eta^2(3 - 2\eta)$ is the function that interpolates properties of the intermediate states in terms of properties of solid and melt and which satisfies conditions $\phi(0) = d\phi(0)/d\eta = d\phi(1)/d\eta = 0$, $\phi(1) = 1$. The order parameter is unambiguously related to volumetric transformation strain (and, consequently, mass density) through Eq. (2).

^{a)}Electronic mail: yshwang@iastate.edu

^{b)}Electronic mail: vlevitas@iastate.edu

Free energy per unit undeformed volume is:^{4,6}

$$\psi = \psi^e + J\tilde{\psi}^\theta + \psi^\theta + J\psi^\nabla; \tilde{\psi}^\theta = A\eta^2(1 - \eta)^2; \quad (4)$$

$$\psi^e = 0.5K\varepsilon_{0e}^2 + \mu\mathbf{e}_e : \mathbf{e}_e; \psi^\theta = H(T/T_{eq} - 1)\phi(\eta); \quad (5)$$

$$\psi^\nabla = 0.5\beta|\nabla\eta|^2, \quad A := 3H(1 - T_c/T_{eq}). \quad (6)$$

Here, ψ^e , ψ^θ , $\tilde{\psi}^\theta$, and ψ^∇ are the elastic, thermal, double-well, and gradient energies, respectively; ρ_0 and ρ are the mass densities in the undeformed and deformed states, respectively, $J = \rho_0/\rho = 1 + \varepsilon_0$, $K(\eta) = K_m + \Delta K\phi(\eta)$, and $\mu(\eta) = \mu_s\phi(\eta)$ are the bulk and shear moduli, $\Delta K = K_s - K_m$, β is the gradient energy coefficient, H is the latent heat, ∇ is the gradient operator in the deformed state, and $T_c = 0.8T_{eq}$ is the melt instability temperature. Using thermodynamic procedure, the following equations for the stress tensor $\boldsymbol{\sigma}$ is obtained:

$$\boldsymbol{\sigma} = \frac{\partial\psi}{\partial\boldsymbol{\varepsilon}} - J^{-1}\nabla\eta \otimes \frac{\partial\psi}{\partial\nabla\eta} = \boldsymbol{\sigma}_e + \boldsymbol{\sigma}_{st};$$

$$\boldsymbol{\sigma}_e = K\varepsilon_{0e}\mathbf{I} + 2\mu\mathbf{e}_e; \boldsymbol{\sigma}_{st} = \left(\psi^\nabla + \tilde{\psi}^\theta\right)\mathbf{I} - \beta\nabla\eta \otimes \nabla\eta, \quad (7)$$

that consists of elastic $\boldsymbol{\sigma}_e$ stress and surface tension at interfaces $\boldsymbol{\sigma}_{st}$, where \otimes designates the dyadic product of vectors. The same procedure leads to the Ginzburg-Landau equation

$$\frac{1}{L}\frac{\partial\eta}{\partial t} = -J^{-1}\frac{\partial\psi}{\partial\eta}\bigg|_{\boldsymbol{\varepsilon}} + \nabla \cdot \left(J^{-1}\frac{\partial\psi}{\partial\nabla\eta} \right)$$

$$= J^{-1}\left\{-\varepsilon_{0t}p_e + 3p_e\Delta\alpha(T - T_{eq})\right\}\frac{\partial\phi}{\partial\eta}$$

$$- J^{-1}\left\{0.5\Delta K\varepsilon_{0e}^2 + \mu\mathbf{e}_e : \mathbf{e}_e + H\left(\frac{T}{T_{eq}} - 1\right)\right\}\frac{\partial\phi}{\partial\eta}$$

$$- 4A\eta(1 - \eta)(0.5 - \eta) + \beta\nabla^2\eta, \quad (8)$$

where L is the kinetic coefficient and $p_e = \boldsymbol{\sigma}_e : \mathbf{I}/3$ is the mean elastic stress. The temperature evolution equation was derived while allowing for thermomechanical coupling, heat of fusion and dissipation rate due to melting

$$c\frac{\partial T}{\partial t} = \nabla \cdot (\kappa\nabla T) + I - 3T(\alpha_m + \Delta\alpha\phi)\frac{\partial p_e}{\partial t} + \left(\frac{\partial\eta}{\partial t}\right)^2/L$$

$$- \left[3p_eT\Delta\alpha\frac{\partial\phi}{\partial\eta} - H\frac{T}{T_{eq}}\frac{\partial\phi}{\partial\eta}\right]\frac{\partial\eta}{\partial t}, \quad (9)$$

where, c is the heat capacity at $p_e = const$, κ is the thermal conductivity, and I is the irradiated laser power.⁷ This system of equations is supplemented by the dynamic equation of motion, $\rho\frac{\partial^2\mathbf{x}}{\partial t^2} = \nabla \cdot \boldsymbol{\sigma}$. The boundary condition for the order parameter η at the surface with the unit normal \mathbf{n} is

$$J\frac{\partial\psi}{\partial\nabla\eta} \cdot \mathbf{n} = \beta\nabla\eta \cdot \mathbf{n} = -\frac{d\gamma}{d\eta}, \quad (10)$$

where $\gamma(\eta) = \gamma_m + (\gamma_s - \gamma_m)\phi(\eta)$, γ_s and γ_m are the solid-vapor and melt-vapor surface energies.

A thin vertical nanolayer with thickness of 25 nm (like in experiments¹ and simulations⁴) irradiated from the right

side by a laser is treated. Lateral surfaces of the nanolayer are stress-free. Since width of a nanolayer is much smaller than the radius of the irradiated spot, the material is under uniaxial strain condition within a heated region. The boundary conditions $\sigma^x = 0$ and $\varepsilon^y = \varepsilon^z = 0$ (i.e., uniaxial straining) for the principle stresses and strains along the axes within a layer (y and z) and normal to a layer (x) are applied.

Equilibrium melting temperature under uniaxial strain. Under the assumption of homogeneous stress-strain and thermal states, equilibrium melting temperature T_{eq}^e is defined from the condition of the equality of free energy before and after melting $\psi(\eta = 1, T_{eq}^e) = \psi(\eta = 0, T_{eq}^e)$. Elastic and thermal energies Eq. (5) contribute to ψ in this case only and $\boldsymbol{\sigma}_{st} = 0$. Elastic strains are determined from the conditions $\sigma^x = 0$ and $\varepsilon^y = \varepsilon^z = 0$ and Hooke's law

$$\varepsilon_e^x = (C - 1)\varepsilon_{in}, \quad C = \frac{9K}{3K + 4\mu}; \quad \varepsilon_e^y = \varepsilon_e^z = -\varepsilon_{in};$$

$$\varepsilon_{0e} = (C - 3)\varepsilon_{in}; \quad e_e^x = \frac{2}{3}C\varepsilon_{in}; \quad e_e^y = e_e^z = -\frac{1}{3}C\varepsilon_{in}. \quad (11)$$

Substitution of these elastic strains in the expression for elastic energy results in its explicit dependence on η . In particular, for $\eta = 1$ and $T = T_{eq}^e$ the elastic energy is

$$\psi_e = B(T_{eq}^e - T_0)^2; \quad (12)$$

$$B = \left(0.5K_s(C - 3)^2 + \frac{2}{3}\mu_s C^2\right)\alpha_s^2. \quad (13)$$

After melting, elastic energy completely relaxes and $\psi(\eta = 0) = 0$. Thus, equality of the free energy before and after melting results in

$$B(T_{eq}^e - T_0)^2 + H(T_{eq}^e/T_{eq} - 1) = 0 \quad (14)$$

and the quadratic equation with respect to T_{eq}^e with the solution

$$T_{eq}^e = \sqrt{\frac{H^2}{T_{eq}^2} - 4BH\left(\frac{T_0}{T_{eq}} - 1\right)}/2B - \left(\frac{H}{2BT_{eq}} - T_0\right).$$

Utilizing the material properties of Al (Ref. 7) and $T_0 = 293.15$ K, we obtain $T_{eq}^e = 898.1$ K, which is 36 K below T_{eq} . Fig. 1 presents a plot of the free energy vs. order parameter for various temperatures while allowing for elastic energy. For the case when size of the sample in y-direction is the same or smaller than the irradiated spot, one has to change stress-strain state to plane strain $\varepsilon^z = 0$ and $\sigma^x = \sigma^y = 0$. In this case,

$$C = \frac{9K_s}{6K_s + 2\mu_s}; \quad B = \left(0.5K_s(2C - 3)^2 + \mu_s\frac{2}{3}C^2\right)\alpha_s^2$$

and $T_{eq}^e = 920.8$ K, which is still 13 K below T_{eq} .

Phase field simulations. Reduction in equilibrium melting temperature does not necessarily mean that the actual melting temperature will be reduced, because melting may be delayed due to difficulties with nucleation or fast heating. To determine the actual melting process, phase field equations are solved numerically with the help of the finite

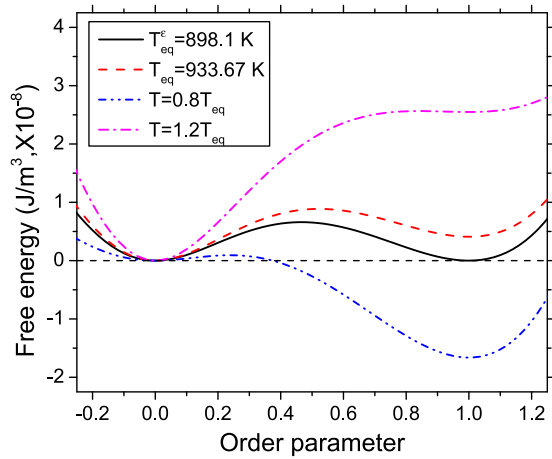


FIG. 1. Free energy plot for aluminum vs. order parameter for uniaxial strain case. Elastic energy increases the total energy of a solid ($\eta = 1$) for any temperature.

element code COMSOL.⁸ The simulation procedure is the same as in Ref. 4, and the details of properties of aluminum, boundary, and initial conditions are summarized in Ref. 7. For 1-D simulation, heating by a short laser pulse with absorbed fluence of 100 J/m^2 and $200 \mu\text{s}$ pulse duration was chosen for slow heating rate, $7.43 \times 10^6 \text{ K/s}$, which does not cause kinetic superheating. Despite the one-side heating, the nanoscale size of the sample and the relatively slow heating rate limit the variation of temperature along the sample by less than 0.1 K. Temperature growth is almost linear until melting occurs followed by a plateau after the initiation of melting due to latent heat (Fig. 2). The temperature of the middle of the sample at the plateau is selected as the melting temperature. Melting temperature in a simulation is 897.5 K, which is very close to $T_{eq}^e = 898.1 \text{ K}$. If mechanical problems and elastic energy are not included in simulation, melting temperature is 933.67 K, i.e., T_{eq} for unstressed case. A similar simulation for the plane strain case resulted in melting at 920.8 K, same as $T_{eq}^e = 920.8 \text{ K}$.

Thus, for relatively slow heating rate, the actual melting temperature is very close to the thermodynamic equilibrium value at the same strains. This is explained by barrierless surface-induced nucleation (premelting) below T_{eq}^e driven by

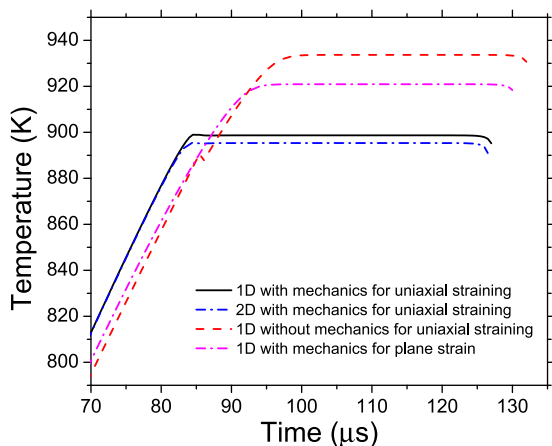


FIG. 2. Evolution of the temperature in the middle of a sample for $Q = 7.43 \times 10^6 \text{ K/s}$.

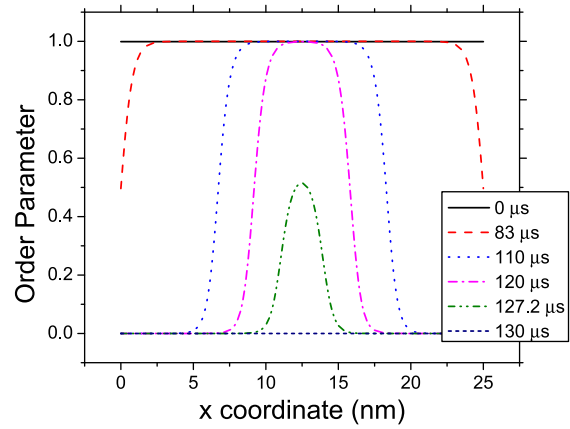


FIG. 3. Evolution of the order parameter within a sample for $Q = 7.43 \times 10^6 \text{ K/s}$.

a reduction in surface energy during melting (Fig. 3). Equilibrium thickness of the molten layer increases with temperature and diverges at T_{eq}^e . That is why, at the chosen heating rate interfaces between solid and liquid propagate to the center of a sample at a temperature close to T_{eq}^e and collide with each other. This collision produces a sudden increase of $|\frac{\partial \eta}{\partial t}|$, which induces a slight temperature drop in the middle of a sample at the end of melting through the term $H \frac{T}{T_{eq}} \frac{\partial \phi}{\partial \eta} \frac{\partial \eta}{\partial t}$ in Eq. (9). The temperature drop in Fig. 2 spreads over the entire sample, since thermal conduction is faster than external heating in this slow-heating case.

Compressive stress along a confined axis increases linearly in time (like temperature) before melting and reaches 2.0 GPa just before melting (Fig. 4). Stress relaxes at the propagating interfaces down to zero. $|\varepsilon_e^y|$ also increases linearly before melting with the strain rate of $2.25 \times 10^2 \text{ s}^{-1}$.

The same problem was solved in 2D formulation for a sample with width of 10 nm and zero displacements and heat flux along axes y and z . Planar solid-melt interfaces propagate to the middle of a sample without any sign of the Grinfeld instability⁹ (waviness) at 895.3 K, i.e., slightly below T_{eq}^e .⁷ Corresponding temperature evolution is presented in Fig. 2.

Competition with kinetic superheating. Since it is known from experiments^{1,2} and simulations^{3,4} that for laser heating

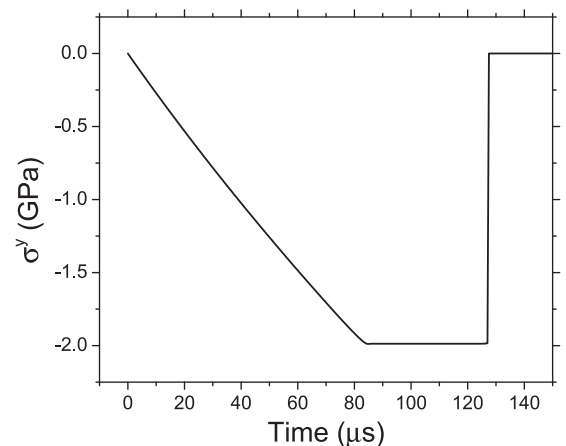


FIG. 4. Evolution of stress σ^y in the middle of a sample for $Q = 7.43 \times 10^6 \text{ K/s}$.

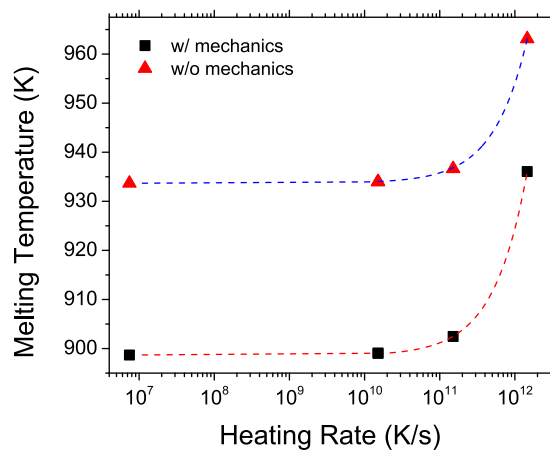


FIG. 5. Melting temperature vs. heating rate.

with $Q > 10^{12}$ K/s melting temperature exceeds T_{eq} , at some point internal stress-induced reduction in melting temperature and kinetic superheating compete with each other. To better understand the initiation of such a competition, laser heating with higher heating rates, 1.51×10^{10} , 1.51×10^{11} , and 1.46×10^{12} K/s, have been simulated (Fig. 5). While below $Q = 1.51 \times 10^{10}$ K/s heating rate does not affect the melting temperature, the triggering of kinetic superheating is visible between $Q = 1.51 \times 10^{10}$ and 1.51×10^{11} K/s, both without and with mechanics effects. However, melting temperature under uniaxial straining at $Q = 1.51 \times 10^{11}$ K/s is still 31 K below T_{eq} . At $Q = 1.46 \times 10^{12}$ K/s, the melting temperature at uniaxial straining becomes $T_{eq} = 936.9$ K, i.e., slightly above T_{eq} .

Note that in experiment the internal stress of 2 GPa (corresponding to $\epsilon_e^y = -0.0181$) may partially relax due to plastic deformation reducing the above effect. The yield strength can be significantly increased and stress relaxation can be significantly suppressed for nanocrystalline and nanosized materials, as well as for high strain rate, which is the case in our problem. Strain rate is found as $\dot{\epsilon}_e^y = -4.57 \times 10^5$ s $^{-1}$ at $Q = 1.51 \times 10^{10}$ K/s and $\dot{\epsilon}_e^y = -4.44 \times 10^7$ s $^{-1}$ at $Q = 1.46 \times 10^{12}$ K/s. Recent molecular dynamics simulations exhibited a lack of plastic deformation above 1 GPa near melting temperature for uniaxial loading at strain rate of 10^8 /s for polycrystalline Al (Ref. 10) and at strain of 0.03 for surface melting of Al.¹¹ Dislocations will be included in future work using the approach developed in Ref. 12.

In summary, in contrast to traditional superheating during intense laser-induced melting, we predicted thermodynamically and confirmed with phase field simulations the possibility of melting of the Al nanolayer 36 K below T_{eq} for the heating rate $Q \leq 1.51 \times 10^{10}$ K/s. It is caused by internal stresses due to thermal strain under constrained uniaxial straining conditions, which relax during melting, producing an additional thermodynamic driving force for melting. Barrierless surface-induced nucleation below these temperatures eliminates kinetic

barriers for such a melting. At higher heating rates, this driving force still persists but kinetic superheating takes over, leading to a significant increase in melting temperature with respect to T_{eq}^e . While we are unaware of similar studies for the reduction in melting temperature due to internal thermal stresses at high heating rate, there were to some extent similar studies under other conditions. Thus, internal stress-induced reduction of the melting temperature at the propagating interface between two solid phases was treated thermodynamically and confirmed experimentally^{13–16} and with PFA.¹⁷ Reduction in melting temperature under nonhydrostatic stresses have been treated thermodynamically^{11,18–20} and using molecular dynamics^{11,20} for Al, and the experiment²¹ for pure helium-4 crystal. There are no contradictions between previous and currently reported phenomena. Our simulations allowed us to suggest an experiment for observation of the reduction in melting temperature. In particular, one subjects a thin Al film of 25 nm thickness (like in Refs. 1 and 2) to heating from one open side by laser irradiation, leading to $Q < 10^{11}$ K/s. It can be, e.g., a combination of 100 J/m^2 absorbed fluence and 100 ns pulse which can generate $Q = 1.51 \times 10^{10}$ K/s. Film can be deposited on a rigid, low-conductive substrate to prevent deformation before melting.

Support from ONR, NSF, Agency for Defense Development and Gyeongsang National University (both South Korea), and ISU was gratefully acknowledged.

¹S. Williamson, G. Mourou, and J. C. M. Li, *Phys. Rev. Lett.* **52**, 2364 (1984).

²B. J. Siwick, J. R. Dwyer, R. E. Jordan, and R. J. Dwayne Miller, *Chem. Phys.* **299**, 285 (2004).

³D. S. Ivanov and L. V. Zhigilei, *Phys. Rev. Lett.* **98**, 195701 (2007).

⁴Y. S. Hwang and V. I. Levitas, *Appl. Phys. Lett.* **103**, 263107 (2013).

⁵V. I. Levitas and K. Samani, *Nat. Commun.* **2**, 284 (2011).

⁶V. I. Levitas and K. Samani, *Phys. Rev. B* **84**, 140103(R) (2011).

⁷See supplementary material at <http://dx.doi.org/10.1063/1.4886799> for details of properties of aluminum, formula for laser power, boundary and initial conditions and 2D solution.

⁸COMSOL Multiphysics Reference Manual (COMSOL, 2014).

⁹M. A. Grinfeld, *Sov. Phys. Doklady* **31**, 831 (1986).

¹⁰A. Gerlich, L. Yue, P. Mendez, and H. Zhang, *Acta Mater.* **58**, 2176 (2010).

¹¹U. Tartaglino and E. Tosatti, *Surf. Sci.* **532–535**, 623 (2003).

¹²V. I. Levitas and M. Javanbakht, *Appl. Phys. Lett.* **102**, 251904 (2013).

¹³V. I. Levitas, B. F. Henson, L. B. Smilowitz, and B. W. Asay, *Phys. Rev. Lett.* **92**, 235702 (2004).

¹⁴V. I. Levitas, *Phys. Rev. Lett.* **95**, 075701 (2005).

¹⁵V. I. Levitas, B. F. Henson, L. B. Smilowitz, and B. W. Asay, *J. Phys. Chem. B* **110**, 10105 (2006).

¹⁶V. I. Levitas, Z. Ren, Y. Zeng, Z. Zhang, and G. Han, *Phys. Rev. B* **85**, 220104 (2012).

¹⁷V. I. Levitas and K. Momeni, *Acta Mater.* **65**, 125 (2014).

¹⁸M. Grinfeld, *Thermodynamic Methods in the Theory of Heterogeneous Systems* (Longman, Sussex, 1991).

¹⁹R. F. Sekerka and J. W. Cahn, *Acta Mater.* **52**, 1663–1668 (2004).

²⁰V. I. Levitas and R. Ravelo, *Proc. Natl. Acad. Sci. U.S.A.* **109**, 13204 (2012).

²¹R. H. Torii and S. Balibar, *Physica B* **194–196**, 971 (1994).